XENON TRANSIENTS SIMULATION USING THE REACTOR CODE DONJON

M.T. Sissaoui, G. Marleau and J. Koclas
Institut de génie nucléaire,
École Polytechnique de Montréal
C.P. 6079, succ. Centre-ville, Montréal,
Québec, CANADA H3C 3A7
email: sissaoui@meca.polymtl.ca

ABSTRACT

The DONJON reactor code has a spatial-kinetic capability used to study the transient behavior of the flux distribution. The xenon transients are simulated in a CANDU reactor using the improved quasistatic method with the help of the Feedback Model which calculates the nuclear properties depending on local parameters for each bundle in the core. The introduction of a new module in DONJON allows the calculation of the xenon and iodine concentrations for each bundle in the core by considering its local conditions.

I. INTRODUCTION

The fission product ^{135}Xe has a large absorption cross section for the thermal neutron. The xenon is formed mostly from the decay of the ^{135}I and only a small fraction results directly from fission. The distributed xenon concentration is now treated differently from the traditional method where the effect of the local parameters is not included. For each bundle, nuclear properties generated by the Feedback Model and depending on the local parameters are used to calculate accurately the ^{135}Xe concentration.[1, 2] The reactivity holdup due to the ^{135}Xe (or xenon load) is very significant in a reactor core. The change in power will affect the xenon concentration. When the reactor is shut-down, the ^{135}Xe concentration builds up from the decay of ^{135}I. In such a case, the buildup of ^{135}Xe is very large and the reactor has to be re-started shortly after a shut-down to be able to compensate the xenon load by withdrawing for example the adjusters in a CANDU reactor. In large reactor core, regional oscillations in the neutron flux are another xenon-induced effect. Because xenon oscillations occur at constant power they may go unnoticed unless the flux distribution is monitored at several points in the reactor.

The goal of our calculation is to assess the effect the local parameters on the distributed xenon concentration during xenon transients for a fixed time averaged bundle burnup. The xenon induced spatial flux oscillations are also studied using the code DONJON. The stability of a CANDU-6 reactor core to xenon oscillations will be examined in 3-D geometry.

II. PROBLEM FORMULATION

The multigroup flux $\phi(\vec{r},t)$ and the delayed precursors $C_j(\vec{r},t)$ for each group j in the time-dependent neutron diffusion equations with G energy groups and J delayed-neutron families are given by the following equations:

$$V^{-1}\frac{\partial}{\partial t}\phi(\vec{r},t) = [A(\vec{r},t) + (1-\beta)B_p(\vec{r},t)]\phi(\vec{r},t) + \sum_{j=1}^{J}\lambda_j\vec{\chi_j}C_j(\vec{r},t) \tag{1}$$

$$\frac{\partial}{\partial t}\vec{\chi_j}C_j(\vec{r},t) = \beta_j B_j(\vec{r},t)\phi(\vec{r},t) - \lambda_j\vec{\chi_j}C_j(\vec{r},t), \qquad j=1,\cdots,J \tag{2}$$

where $A(\vec{r},t) = \nabla.D(\vec{r},t)\nabla - S(\vec{r},t)$, $B_p(\vec{r},t) = \vec{\chi_p}\vec{F^t}(\vec{r},t)$ and $B_j(\vec{r},t) = \vec{\chi_j}\vec{F^t}(\vec{r},t)$. $D(\vec{r},t)$, $S(\vec{r},t)$ and $\vec{F}(\vec{r},t)$ are respectively the diagonal diffusion coefficients matrix $(g\times g)$, total removal minus scattering matrix $(g\times g)$ and the neutron production operator. The prompt neutron fission spectrum $\vec{\chi_p}$ can differ from the delayed neutron fission spectra $\vec{\chi_j}$ $(g\times 1)$. λ_j is the decay constant and β_j the delayed neutron fraction. The total delayed fraction is $\beta = \sum_{j=1}^{J}\beta_j$ and V^{-1} is the diagonal inverse velocity matrix $(g\times g)$.

The xenon and iodine concentrations are space and time dependent. The equations specifying the time dependence of these concentrations are given by

$$\frac{\partial}{\partial t}N^i(\vec{r},t) = -\lambda_i N^i(\vec{r},t) + \gamma_i\Sigma_f(\vec{r},t)\phi(\vec{r},t) \tag{3}$$

$$\frac{\partial}{\partial t}N^x(\vec{r},t) = \lambda_i N^i(\vec{r},t) - \lambda_x N^x(\vec{r},t) + \gamma_x\Sigma_f(\vec{r},t)\phi(\vec{r},t) - \sigma_x(\vec{r},t)N^x(\vec{r},t)\phi(\vec{r},t) \tag{4}$$

where $N^x(\vec{r},t)$ and $N^i(\vec{r},t)$ are the space-time dependent concentrations of xenon and iodine. $\Sigma_f(\vec{r},t)$ is the fission macroscopic cross section and $\sigma_x(\vec{r},t)$ the xenon microscopic absorption cross section. λ_x and λ_i are the decay constant and γ_x and γ_i are the average direct yield per fission of xenon and iodine respectively. The metastable state of the xenon is not included in these equations.[3]

For the steady state, the equilibrium values of the xenon and iodine are

$$N^i_\infty(\vec{r}) = \frac{\gamma_i\Sigma_f(\vec{r})\phi(\vec{r})}{\lambda_i} \tag{5}$$

$$N^x_\infty(\vec{r}) = \frac{(\gamma_i+\gamma_x)\Sigma_f(\vec{r})\phi(\vec{r})}{\lambda_x + \sigma_x\phi(\vec{r})} \tag{6}$$

Eqs. (5) and (6) shows that at equilibrium the concentrations are flux-dependent and distributed in the reactor.

The time-dependent neutron diffusion equation is solved using the improved quasistatic methods.[4, 5] This method is based on the separation of the temporal and spatial variables in the flux. The improved quasistatic methods splits the flux $\phi(\vec{r},t) = \varphi(\vec{r},t)T(t)$ in the time-dependent diffusion equation into a product of a slowly varying shape function $\varphi(\vec{r},t)$ equation by an amplitude function $T(t)$. This factorization splits the time dependent flux distribution given by the time dependent diffusion equations into a point

kinetic equations, precursor equation and a shape function equation. The shape function leads to an implicit equation of $\varphi(\vec{r},t)$. The point kinetic equations are found by applying a functional to the time dependent diffusion equation with a factored flux. This functional is a weighted integral over the volume and a summation over all energy-groups. The discretization of the spatial and temporal variables were made using respectively the nodal collocation method and the finite element method.[6] After the discretization of the spatial variable $\vec{r}$ was performed the shape function $\varphi(t)$ and the nuclear cross section matrices $A(t)$, $B_j(t)$ and $B_p(t)$ are assumed to have a linear variation over the macro-time step $\Delta t = t_n - t_{n-1}$.

The equations describing the xenon and iodine variation as function of the local flux (bundle) $\phi = \phi(t_{n-1})$ and the time step Δt are

$$N^i(t_n) = N^i(t_{n-1})exp(-\lambda_i\Delta t) + N^i_\infty[1 - exp(-\lambda_i\Delta t)] \tag{7}$$

$$\begin{aligned} N^x(t_n) = {} & N^x(t_{n-1})exp(-(\sigma_x\phi + \lambda_x)\Delta t) + N^x_\infty[1 - exp(-(\sigma_x\phi + \lambda_x)\Delta t)] \\ & +\lambda_i\frac{(N^i(t_{n-1}) - N^i_\infty)}{\lambda_x - \lambda_i + \sigma_x\phi}[exp(-(\sigma_x\phi + \lambda_x)\Delta t) - exp(-\lambda_i\Delta t)] \end{aligned} \tag{8}$$

An analytic solution for each mesh point (bundle) is used to take into account the changes of theses concentrations over a time step.[7, 8]

III. DONJON CALCULATION

The xenon transient following a variation in reactor power vary spatially as the ^{135}I distribution is directly proportional to the flux distribution for a reactor core at equilibrium. A module implemented in DONJON is used to treat explicitly the spatial dependence of the ^{135}Xe and ^{135}I concentrations during transients.

The starting conditions correspond to a reactor with xenon and iodine concentrations at equilibrium for a given power level. To take into account the changes over a time step, this module update theses concentrations using an analytic solution for each mesh point (bundle) (see Eqs. (7) and (8)). The xenon reactivity transients for a CANDU reactor are performed using a three-dimensional diffusion calculation. The effect of inserting reactivity control devices in a CANDU reactor is taken into account by using the incremental cross sections obtained from a 3-D supercell calculation.[9] The cross sections are defined by averaging the lattice cross sections over the burnup range. Each bundle has an average cross sections determined by

$$\Sigma(\vec{L}) = \frac{1}{B_{out} - B_{in}}\int_{B_{in}}^{B_{out}} \Sigma(B,\vec{L})dB \tag{9}$$

where the vector $\vec{L}$ represents the local parameters, B_{in} the burnup at the beginning of the residence time and B_{out} the end. Three uniform burnup zones are defined to ensure a critical reactor. For our test we run a full core time average calculation which was solved by using mesh-centered finite-difference method. For the point kinetic equations the Kaps and Rentrop integration scheme is used.[4]

The xenon load following shutdown from full power (2180 MW) using different macro-time steps was studied. The transients were followed for about one minute (see Figure 1). The results obtained show a cutoff in the xenon load due to numerical errors when macro-time steps shorter than 5 seconds are used. To avoid these errors a larger macro-time steps must be considered.

The following xenon transients will be studied such as shutdowns from various power levels, power setback from full power and xenon spatial oscillations. These studies will allow us to draw conclusions on the real effect of the local parameters on xenon transients.

III.1 XENON LOAD

For the reference steady state calculations the fuel temperature and the power are at their nominal values and only the xenon correction is considered. The adjusters are fully inserted and the liquid zone controller are half filled. This results in a xenon load at full reactor power of 27.4 mk. When in addition to the xenon correction the local parameters (fuel temperature and the power history) effect are considered the xenon load is slightly affected and is equal to 27.0 mk. These steady state calculations show a different distribution of xenon concentration compared to the traditional method where no local parameters are included.

For the xenon load calculations, a 60 s macro-time step is used for both iodine and xenon evolution and the equations of the quasistatic solution. When the reactor power is set back from full power to a lower level the xenon concentration is affected. For the first xenon transient tests, we covered the first hour of the reactor shut-down to evaluate the time before the xenon load reaches 15.0 mk corresponding to the reactivity worth of the adjuster. Because of the different distribution of xenon concentration due to the local parameters it takes approximately one minute and a half more (36.8 mn) to reach a xenon load of 15.0 mk and poison out the reactor.

The xenon reactivity (adjuster fully in the core) versus time after power setback to 0%, 20%, 40%, 60% and 80% of full power (FP) with local parameters ($\rho_{X,L}$) are shown in Figure 2. During these power transients the local parameters were not modified. The case with no local parameters (ρ_X) over-estimates the xenon load in the reactor and this effect dependent on the power setback. The maximum and minimum deviation in reactivity $\Delta\rho = \rho_{X,L} - \rho_X$ between the two cases are given in Table 1.

In the case where the adjusters are removed from the core, the xenon reactivity transients after shutdown from 100 %, 80%, 60%, 40% and 20% of full power with local parameters are shown in figure Figure 3. As we can see in general from Table 2 the effect of the local parameters reduce the worth of the xenon load.

Xenon transients after startup to 20%, 40%, 60%, 80% and 100 % of full power was simulated during 60 hours are shown in Figure 4. The local parameters are taken into account and the adjuster are fully in the core. Table 2 shows that the maximum deviation reached is about 0.4 mk at 100% of full power.

III.2 XENON OCSILLATIONS

Thermal reactors core operating at high power levels are susceptible to oscillations in power distribution that are associated with xenon spatial distribution. A large core size

(dimensions large compared to the neutron migration length) enhances the possibility of xenon instability. In CANDU-6 reactor the spatial xenon oscillation are possible when the zone control system to counteract the xenon oscillation is not available. Various methods have been used to study the xenon-induced spatial power oscillations such as the λ-modes.[10] The stability of the CANDU-6 has been studied with the help of DONJON code in 3-D geometry to determine the threshold power to xenon oscillation below which the reactor core is stable. At threshold the spatial oscillation are stable and do not either grow or decay. These xenon oscillations are unstable if the total power is above the threshold power and damp if below. Two perturbations modes were analyzed, the first azimuthal top-to-bottom and side-to-side. Initially all the zone control units are 50 % filled with light water (steady state reactor). To introduce the instability in the system, the liquid zone controller level are increased to 70 % in one region and in the same time decreased to 30 % for another region. The total power is maintained constant during the transient. The iodine and xenon concentrations and the quasistatic solutions are computed using a $\Delta t = 120$ s macro-time step.

The results obtained for the maximum bundle power are normalized to the average bundle power in the reactor. For a top-to-bottom perturbation with local parameters Figure 5 shows a reactor stable to spatial oscillations at 43 % of full power. As shown in Figure 6 and 7, these power oscillations are damp below the threshold at 42 % FP and unstable above the threshold at 44 % FP.

The fact of not considering the local parameters has decreased the threshold power for the top-to-bottom perturbation and this effect is about 5 % of full power and increased by 2 % for the side-to-side perturbation (see Table 4). The difference in threshold power is due to the overall power flattering in the core when the local parameters are considered. We note that when applying the local parameter correction, the maximum bundle power generally decreases (see Figure 8 and 9) indicating that the fuel temperature correction reduces the maximum bundle power. Table 5 shows the power reduction (first maximal amplitude reached) obtained for different power levels of the reactor.

The period of oscillation with local parameters for several power levels are summarized in Table 6. Theses observed periods are found to be decreasing with the reactor core power level.

IV. CONCLUSION

The DONJON reactor code has been extended to simulate the xenon transients by implementing a new module which treat explicitly the spatial dependence of ^{135}Xe and ^{135}I concentrations during transients. This code has been used to investigate the effect of the local parameters on the xenon load and the stability of xenon-induced spatial oscillations. A three-dimensional geometry representing CANDU-6 has been used. The results have shown that the absence of the local parameter correction has relatively little effect on xenon load. On the contrary, the xenon induced spatially uncontrolled power oscillations are affected by local parameters and it may be important to take it into account in reactor analysis.

REFERENCES

[1] M.T. Sissaoui, G. Marleau and D. Rozon, "Accounting For Actinide Burnup History in CANDU Reactor Simulation", *Advances In Nuclear Fuel Management II*, Myrtle beach, South Carolina, March 23-26, 1997.

[2] M.T. Sissaoui and G. Marleau, "Application of the Feedback Model for the History Base Using DRAGON", *19th CNS Simulation Symposium*, Hamilton, Canada, October 16-17, 1995.

[3] M. Salvatore, D.A. Jenkins, B. Rouben, C. Newman and E. Young, "Simulating Xenon Transients Via the History Based Local Parameters Methodology Including the Metastable State of Xenon-135", *17th CNS Simulation Symposium*, Kingston, Canada, August 16-18, 1992.

[4] M.T. Sissaoui, J. Koclas and A. Hébert, *Ann. Nucl. Energy*, **22**, 763, 1995.

[5] J. Koclas, M.T. Sissaoui and G. Marleau, *Ann. Nucl. Energy*, **24**, 1223, 1997.

[6] A. Hébert, *Ann. Nucl. Energy*, **10**, 527, 1987.

[7] D. Rozon, *Introduction à la cinétique des réacteur nucléaire*, École Polytechnique de Montréal, Montréal, Canada, 1992.

[8] A. Qaddouri, *La détermination d'une séquence d'extraction et d'insertion des barres de compensation dans un réacteur CANDU*, M.sc.A. École Polytechnique de Montréal, Montréal, Canada, 1992.

[9] G. Marleau, R. Roy and B. Arsenault, "Simulation of Reactivity Control Devices in a CANDU-6 Reactor Using DRAGON", *CNS Proceedings of the 1994 Nuclear Simulation Symposium*, Pembroke, Canada, 1994.

[10] M. Mamourian and P. Akhtar, "Analysis of Xenon-Induced Power Oscillations with λ-modes", *17th Annual CNA/CNS International conference*, Montreal, Canada, June 5-8, 1977.

Table 1: Deviation in xenon load following step power reductions

Power setback from full power (100%) to (%)	Minimum $\Delta\rho$ (mk)	Maximum $\Delta\rho$ (mk)
0	0.4	2.8
20	0.4	1.3
40	0.4	0.7
60	0.4	0.6
80	0.4	0.5

Table 2: Deviation in xenon load after shutdown from various power levels

Power level before Shutdown (%)	Minimum $\Delta\rho$ (mk)	Maximum $\Delta\rho$ (mk)
20	0.2	0.7
40	0.1	1.3
60	0.1	1.9
80	0.6	2.9
100 (full power)	-6.5	5.4

Table 3: Deviation in xenon load after startup to various power levels

Power startup to (%)	Maximum $\Delta\rho$ (mk)
20	0.15
40	0.06
60	0.03
80	0.05
100 (full power)	0.40

Table 4: Threshold to xenon induced power oscillations

Perturbation	Threshold power (with local parameters) (%)	Threshold power (without local parameters) (%)
Top-to-bottom	43	38
Side-to-side	53	55

Table 5: Maximum bundle power for top-to-bottom perturbation

Power (%)	Maximum bundle power with local parameter	Maximum bundle power without local parameter	Power reduction (%)
50	1.5388	1.5896	3.8
60	1.6067	1.6949	5.5
70	1.6723	1.7979	7.0
80	1.7421	1.8960	8.1
90	1.8024	1.9704	8.5
100	1.8614	2.0379	8.7

Table 6: Oscillations periods of CANDU-6 uncontrolled

Power (%)	Top-to-bottom oscillations period (hour)	Side-to-side oscillations period (hour)
50	23.76	-
60	22.26	22.50
70	21.50	20.96
80	21.20	20.20
90	21.13	18.96
100	18.73	18.53

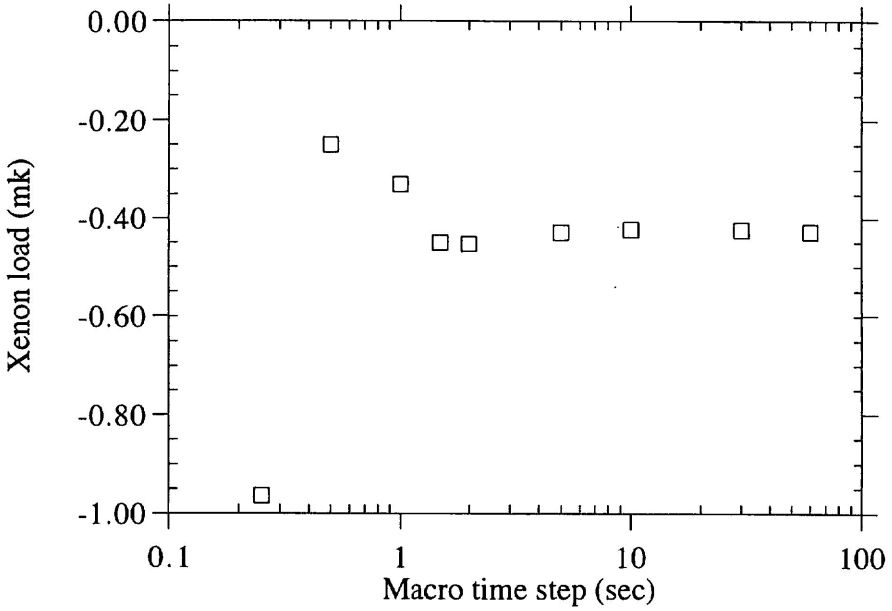

Figure 1: Xenon load after 60s with different macro-time step

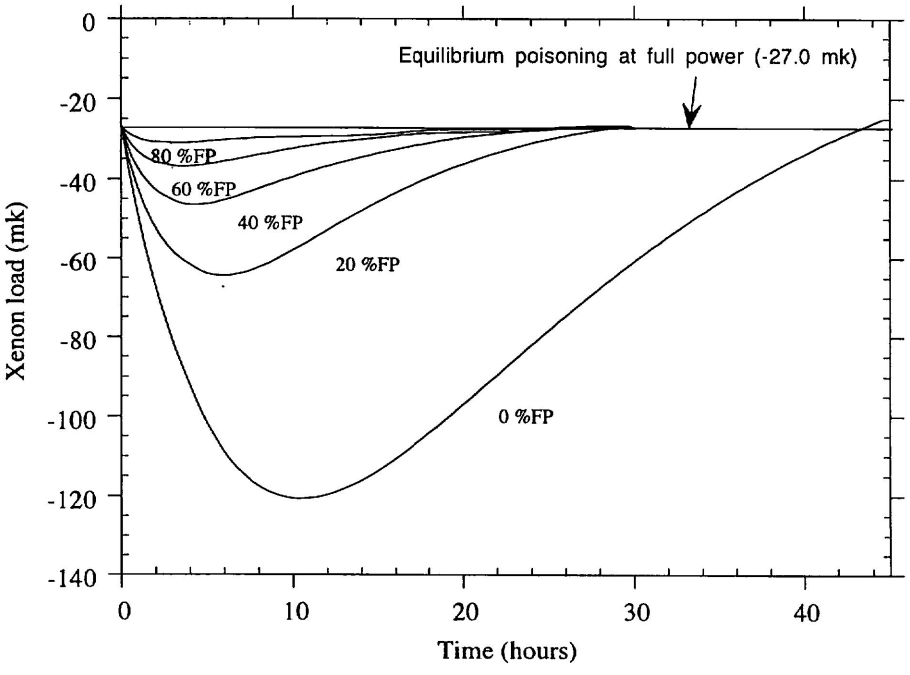

Figure 2: Xenon load following power step reductions

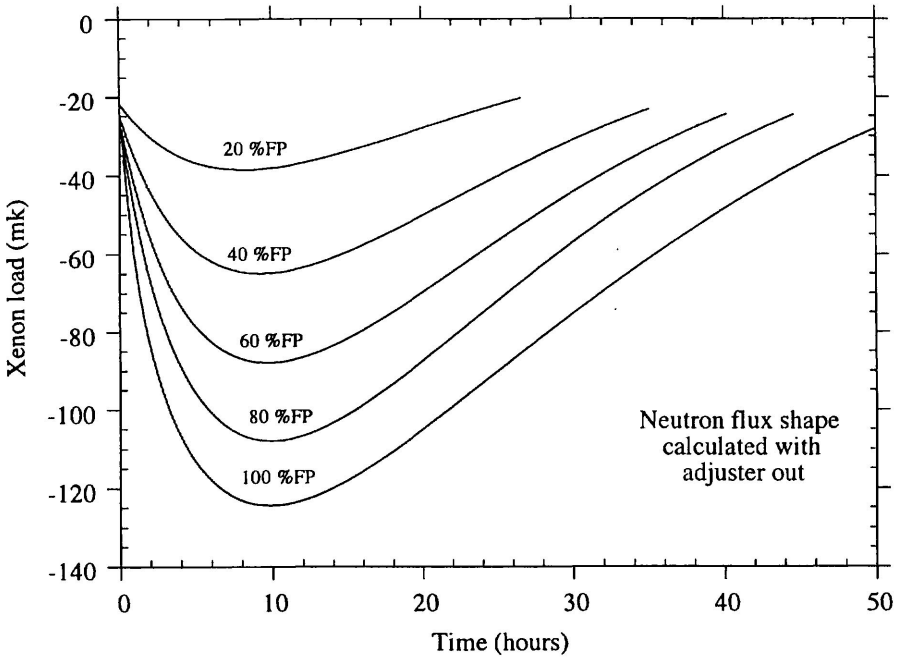

Figure 3: Xenon load after shutdown from various power levels

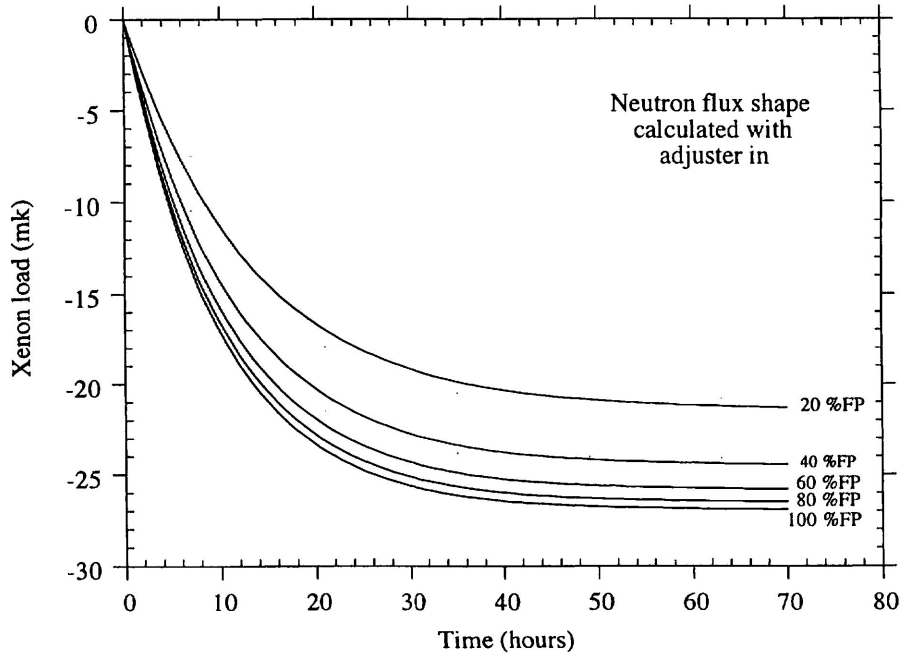

Figure 4: Xenon load after startup to various power levels

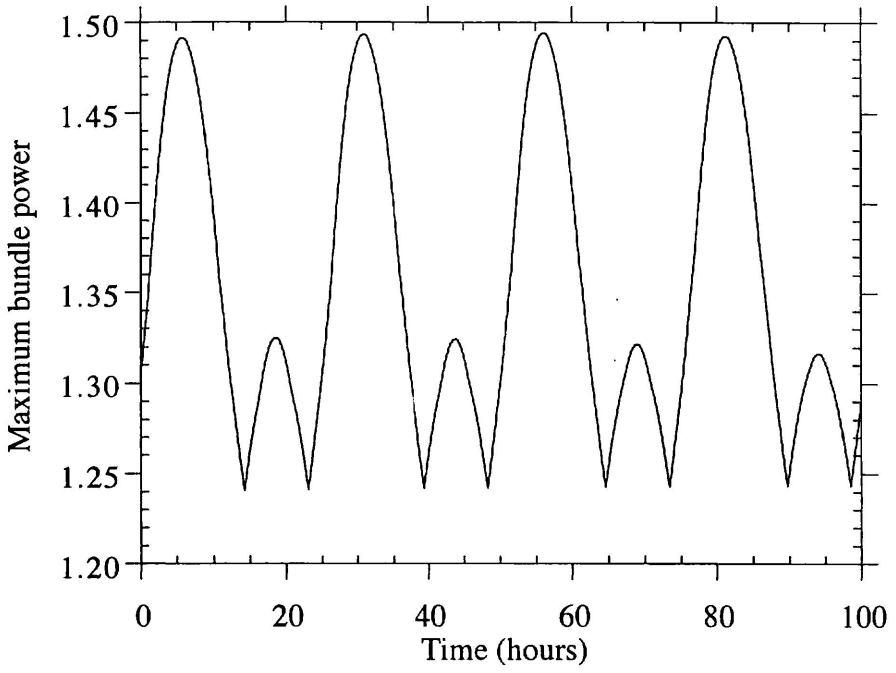

Figure 5: Maximum bundle power at threshold (43% FP) for top-to-bottom perturbation

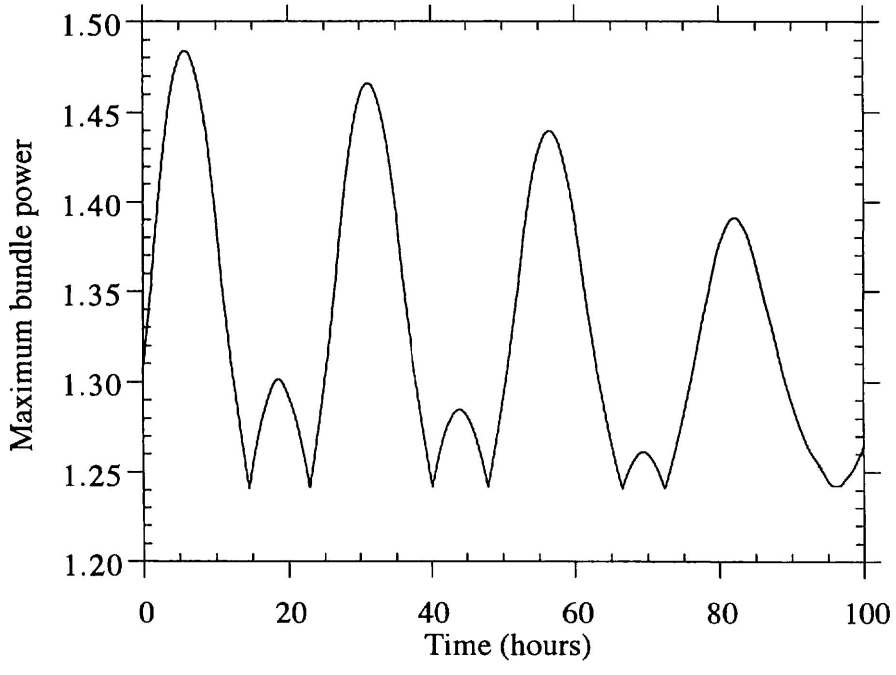

Figure 6: Maximum bundle power below threshold (42% FP) for top-to-bottom perturbation

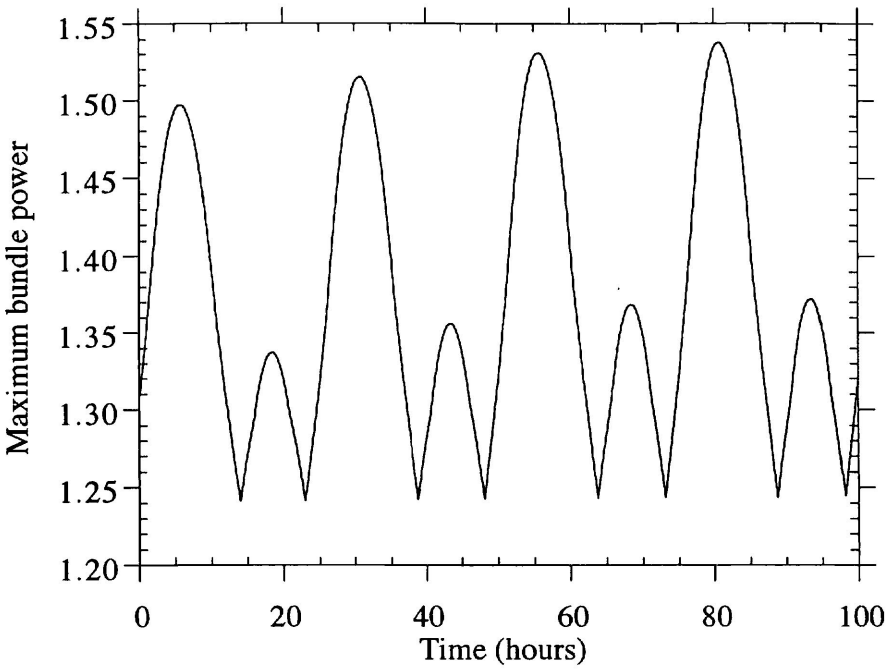

Figure 7: Maximum bundle power above threshold (44% FP) for top-to-bottom perturbation

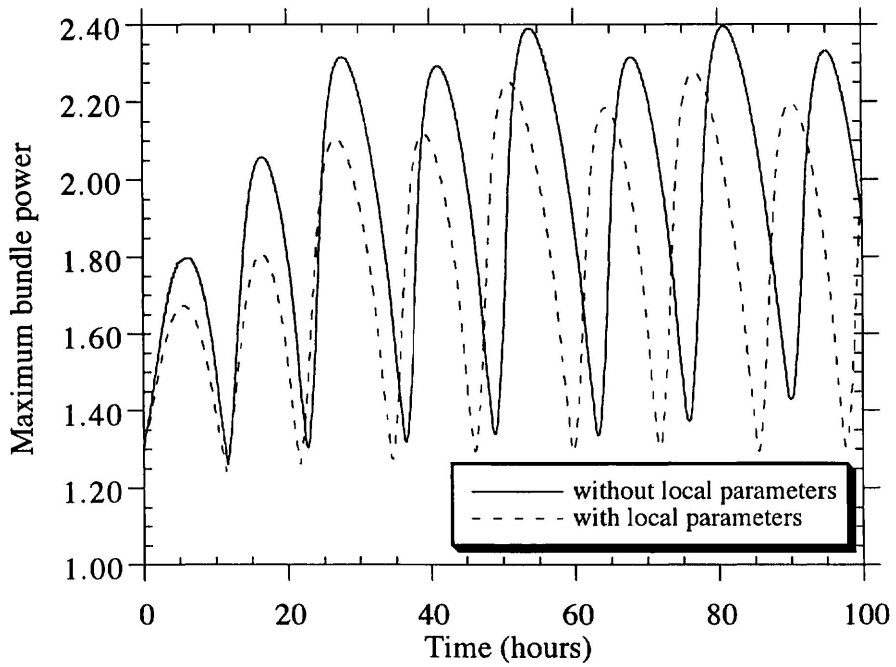

Figure 8: Maximum bundle power at 70 % FP for top-to-bottom perturbation

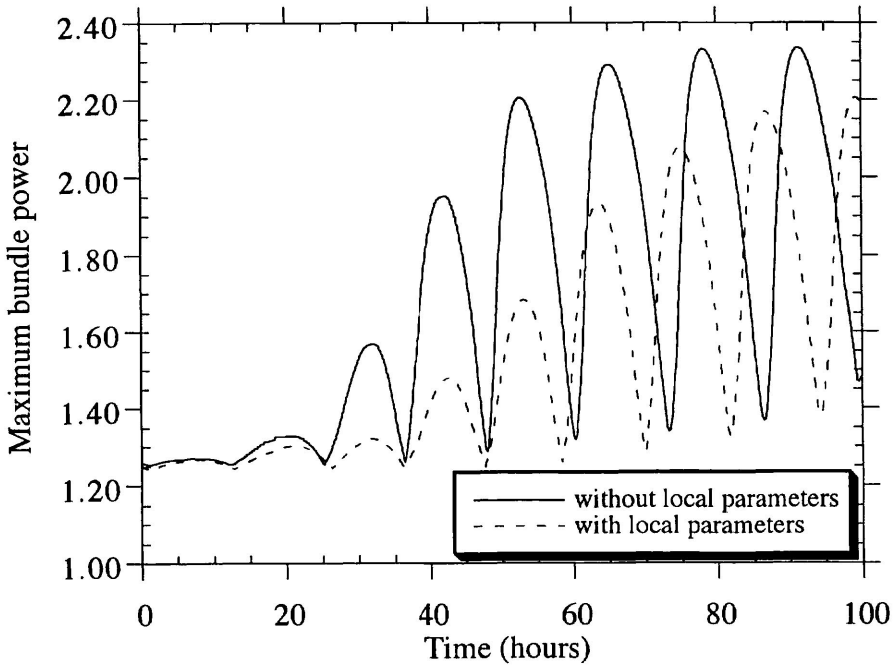

Figure 9: Maximum bundle power at 70 % FP for side-to-side perturbation